Published in final edited form as:
Eur J Pharmacol. 2012 December 5; 696(0): 18–27. doi:10.1016/j.ejphar.2012.09.013.

Interaction of HM30181 with P-glycoprotein at the murine blood-brain barrier assessed with positron emission tomography

Florian Bauer[a,1], **Thomas Wanek**[b,1], **Severin Mairinger**[a,b,c], **Johann Stanek**[b,c], **Michael Sauberer**[b], **Claudia Kuntner**[b], **Zahida Parveen**[d], **Peter Chiba**[d], **Markus Müller**[c], **Oliver Langer**[b,c,*], and **Thomas Erker**[a]

[a]Department of Medicinal Chemistry, University of Vienna, Vienna, Austria

[b]Health & Environment Department, Biomedical Systems, AIT Austrian Institute of Technology GmbH, Seibersdorf, Austria

[c]Department of Clinical Pharmacology, Medical University of Vienna, Vienna, Austria

[d]Institute of Medical Chemistry, Medical University of Vienna, Vienna, Austria

Abstract

HM30181, a potent and selective inhibitor of the adenosine triphosphate-binding cassette transporter P-glycoprotein (Pgp), was shown to enhance oral bioavailability and improve antitumour efficacy of paclitaxel in mouse tumour models. In search for a positron emission tomography (PET) radiotracer to visualise Pgp expression levels at the blood-brain barrier (BBB), we examined the ability of HM30181 to inhibit Pgp at the murine BBB. HM30181 was shown to be approximately equipotent with the reference Pgp inhibitor tariquidar in inhibiting rhodamine 123 efflux from CCRF-CEM T cells (IC_{50}, tariquidar: 8.2±2.0 nM, HM30181: 13.1±2.3 nM). PET scans with the Pgp substrate (*R*)-[^{11}C]verapamil in FVB wild-type mice pretreated i.v. with HM30181 (10 or 21 mg/kg) failed to show significant increases in (*R*)-[^{11}C]verapamil brain uptake compared with vehicle treated animals. PET scans with [^{11}C]HM30181 showed low and not significantly different brain uptake of [^{11}C]HM30181 in wild-type, *Mdr1a/b*$^{(-/-)}$ and *Bcrp1*$^{(-/-)}$ mice and significantly, i.e. 4.7-fold (P<0.01), higher brain uptake, relative to wild-type animals, in *Mdr1a/b*$^{(-/-)}$*Bcrp1*$^{(-/-)}$ mice. This was consistent with HM30181 being at microdoses a dual substrate of Pgp and breast cancer resistance protein (Bcrp). *In vitro* autoradiography on low (EMT6) and high (EMT6Ar1.0) Pgp expressing murine breast tumour sections showed 1.9 times higher binding of [^{11}C]HM30181 in EMT6Ar1.0 tumours (P<0.001) which was displaceable with unlabelled tariquidar, elacridar or HM30181 (1 μM). Our data suggest that HM30181 is not able to inhibit Pgp at the murine BBB at clinically feasible doses and that [^{11}C]HM30181 is not suitable as a PET tracer to visualise cerebral Pgp expression levels.

Keywords

P-glycoprotein; blood-brain barrier; HM30181; tariquidar; positron emission tomography; microdosing

[*]*Corresponding author:* Tel.: +43-0-50550-3496; fax: +43-0-50550-3473. oliver.langer@ait.ac.at.
[1]These authors contributed equally to this work.

Europe PMC Funders Author Manuscripts

1. Introduction

The adenosine triphosphate-binding cassette (ABC) transporter P-glycoprotein (Pgp) is highly expressed in the luminal membrane of brain capillary endothelial cells forming the blood-brain barrier (BBB) where it restricts brain distribution of its substrates by active ATP-driven efflux transport (Löscher and Potschka, 2005). Many clinically used drugs are substrates of Pgp and therefore possess low brain uptake. Pgp-mediated efflux transport at the BBB has been implicated in central nervous system (CNS) drug resistance, notably in epilepsy (Brandt et al., 2006; van Vliet et al., 2006), stroke (Spudich et al., 2006), depression (O'Brien et al., 2012) and brain tumours (Agarwal et al., 2011). A promising strategy to overcome CNS drug resistance may be cotreatment of resistant patients with third-generation Pgp modulators, such as tariquidar (XR9576) or elacridar (GF120918), which may increase drug concentration levels, particularly in brain regions exhibiting transporter overexpression, by inhibition of Pgp efflux transport (Potschka, 2012). As Pgp inhibition may be associated with CNS side effects, it may be desirable to assess the functional status of Pgp at the BBB in individual patients before initiation of treatment with Pgp modulators so that only those patients are treated, whose resistance is caused by a transporter-mediated mechanism.

A powerful tool to assess Pgp function at the BBB of animals and humans is the non-invasive molecular imaging technique positron emission tomography (PET) using radiolabelled Pgp substrates, such as racemic [^{11}C]verapamil, (*R*)-[^{11}C]verapamil or [^{11}C]-*N*-desmethyl-loperamide (Kannan et al., 2009; Mairinger et al., 2011). However, all these probes are high-affinity substrates of Pgp and consequently possess very low brain uptake. They are therefore not ideal to detect regionally increased Pgp activity at the BBB as such an increase in transporter activity would lead to a further reduction in PET imaging signal which is very difficult to detect against a low background of radiotracer uptake in the brain (Bankstahl et al., 2011).

As an alternative to Pgp substrate radiotracers, radiolabelled Pgp inhibitors, such as [^{11}C]laniquidar (Luurtsema et al., 2009), [^{11}C]elacridar (Dörner et al., 2009; Kawamura et al., 2011) and [^{11}C]tariquidar (Bauer et al., 2010; Kawamura et al., 2010) have been proposed. It was expected that such probes would bind to Pgp at the BBB without being transported and thereby allow for mapping of Pgp density leading to increased PET imaging signals in brain regions overexpressing Pgp. However, contrary to these initial expectations all radiolabelled Pgp inhibitors characterised to date were shown to possess very low brain uptake in rodents, most likely because they were recognised by breast cancer resistance protein (Bcrp), another member of the ABC transporter family expressed at the BBB, as substrates (Kannan et al., 2011; Mairinger et al., 2011).

HM30181 (*N*-(2-(2-(4-(2-(6,7-dimethoxy-3,4-dihydroisoquinolin-2(1*H*)-yl)ethyl)phenyl)-2*H*-tetrazol-5-yl)-4,5-dimethoxyphenyl)-4-oxo-4*H*-chromene-2-carboxamide, Fig. 1), which is a close structural analogue of tariquidar, is currently developed by Hanmi Pharmaceuticals Co. Ltd (Republic of Korea) as a Pgp modulator (Kim et al., 2012; Kwak et al., 2010). It has been shown that HM30181 is approximately 24 times more potent than tariquidar in inhibiting Pgp-mediated transport of rhodamine 123 from 293FRT-MDR1 cells and at least 20 times less potent than tariquidar in inhibiting ATPase activity in BCRP enriched membrane vesicles (Kwak et al., 2010). It has also been shown that oral treatment with HM30181 (10 mg/kg) increases bioavailability of the chemotherapeutic drug paclitaxel, which is a Pgp substrate, from 3% to 41% in rats (Joo et al., 2008; Kwak et al., 2010). Based on these reported properties, HM30181 appears as a promising candidate compound for development of a PET tracer for visualisation of Pgp density at the BBB, which is expected to bind with higher affinity to Pgp and to be less

likely effluxed by Bcrp at the BBB than [^{11}C]tariquidar. In the present work, we assessed the suitability of carbon-11-labelled HM30181, as compared with previously developed [^{11}C]tariquidar (Bauer et al., 2010), to visualise Pgp expression levels at the murine BBB with PET and also studied the ability of HM30181 to inhibit Pgp at the murine BBB.

2. Material and methods

2.1. General

Chemicals were purchased from Sigma-Aldrich Chemie GmbH (Schnelldorf, Germany), Merck (Darmstadt, Germany) or Apollo Scientific Ltd (Bredbury, UK) at analytical grade and used without further purification. The mesylate of HM30181 was synthesised following a published procedure (Bang et al., 2005). For i.v. administration to animals, HM30181 mesylate was freshly dissolved on each experimental day in 5% (w/v) aqueous (aq.) glucose solution, containing 20 μl 0.01 M aq. HCl and injected at a volume of 4 ml/kg (Bang et al., 2005). Tariquidar dimesylate and elacridar hydrochloride were synthesised following literature procedures (Bauer et al., 2010; Dörner et al., 2009). For *in vitro* autoradiography, elacridar hydrochloride was dissolved in 20% (v/v) aq. ethanol solution, HM30181 mesylate in 5% (w/v) aq. glucose solution (containing 20 μl 0.01 M aq. HCl) and tariquidar dimesylate in 2.5% (w/v) aq. glucose solution immediately prior use. [^{11}C]Methane was produced *via* the ^{14}N(p,α)^{11}C nuclear reaction by irradiation of nitrogen gas containing 10% hydrogen using a PETtrace cyclotron equipped with a methane target system (GE Healthcare, Uppsala, Sweden). [^{11}C]Methyl iodide was prepared in a TracerLab FXC Pro synthesis module (GE Healthcare) and converted into [^{11}C]methyl triflate by passage through a column containing silver-triflate impregnated graphitised carbon. ^{1}H- and ^{13}C-NMR spectra were recorded on a Bruker Advance DP × 200 (200 and 50 MHz respectively). Chemical shifts are reported in δ units (ppm) relative to Me_4Si- or solvent residual line as internal standard (s, bs, d, m, C_q for singlet, broad singlet, doublet, multiplet and quaternary carbon, respectively) and *J* values are reported in Hertz. Mass spectra (MS) were obtained with a Shimadzu (GC-17A; MS-QP5050A) spectrometer. Elemental analysis was performed on a Perkin Elmer 2400 CHN Elemental Analyser.

2.2. Animals

Female *Mdr1a/b*$^{(-/-)}$, *Bcrp1*$^{(-/-)}$ and *Mdr1a/b*$^{(-/-)}$*Bcrp1*$^{(-/-)}$ mice with a FVB genetic background were obtained from Taconic (Germantown, USA). Female FVB wild-type mice were either purchased from Taconic or Charles River (Sulzfeld, Germany). The study was approved by the local animal welfare committee and all study procedures were performed in accordance with the Austrian Animal Experiments Act. All efforts were made to minimise both the suffering and the number of animals used in this study.

2.3. Chemistry and radiochemistry

2.3.1. (E)-N'-(4-(Benzyloxy)-5-methoxy-2-nitrobenzylidene)-4-methylbenzenesulfonohydrazide (1)—To a stirred suspension of 4-methylbenzenesulfonohydrazide (0.64 g, 3.44 mmol) in ethanol (7 ml), 4-(benzyloxy)-5-methoxy-2-nitrobenzaldehyde (1.01 g, 3.52 mmol) suspended in ethanol (23 ml) was added. The resulting mixture was stirred under reflux for 1 h. After cooling to room temperature water (100 ml) was added. The precipitate was collected by vacuum filtration to obtain title compound **1** as a yellow solid (1.37 g, 87%). The product was used without further purification in the next reaction step.

^{1}H-NMR (d_6-DMSO): δ 2.36 (s, 3H, CH_3), 3.89 (s, 3H, OCH_3), 5.22 (s, 2H, OCH_2), 7.16 (s, 1H), 7.32 – 7.51 (m, 7H), 7.72 (s, 1H), 7.81 (d, 2H, *J*=8.2 Hz), 8.36 (s, 1H), 11.77 (s, 1H, NH). ^{13}C-NMR (d_6-DMSO): δ 21.0 (CH_3), 56.1 (OCH_3), 70.4 (OCH_2), 108.5 (CH), 109.0

(CH), 123.0 (C_q), 127.3 (CH), 128.0 (CH), 128.2 (CH), 128.5 (CH), 129.7 (CH), 135.9 (C_q), 136.0 (C_q), 140.6 (C_q), 142.9 (CH), 143.7 (C_q), 148.5 (C_q), 153.0 (C_q). MS *m/z* 107 (7%), 92 (14%), 91 (100%), 65 (30%), 63 (11%), 51 (9%).

2.3.2. 2-(4-(5-(4-(Benzyloxy)-5-methoxy-2-nitrophenyl)-2H-tetrazol-2-yl)phenethyl)-6,7-dimethoxy-1,2,3,4-tetrahydroisoquinoline (2)—To an ice cooled suspension of 6,7-dimethoxy-2-(4-aminophenethyl)-1,2,3,4-tetrahydroisochinoline (Ashworth et al., 1996; Sharp et al., 1998) (0.65 g, 2.08 mmol) in 50% aq. ethanol (3.5 ml), concentrated HCl (0.56 ml) was added dropwise. After addition of $NaNO_2$ (0.17 g, 2.42 mmol) in water (0.88 ml) the resulting mixture was stirred at 0°C for 15 min and then cooled to −15 °C. Compound **1** (0.95 g, 2.07 mmol) in pyridine (12 ml) was added over a period of 5 min. The reaction mixture was stirred at −15 °C for 3 h and then at room temperature overnight. The slurry was acidified with aq. HCl (1 M, 170 ml) and extracted with dichloromethane. The organic phase was washed with aq. HCl (1 M), water, saturated aq. $NaHCO_3$ solution and brine, dried over Na_2SO_4 and concentrated under reduced pressure. The crude product was purified by recrystallisation from toluene to obtain title compound **2** as orange solid (1.11 g, 86%).

^{1}H-NMR ($CDCl_3$): δ 2.78 – 3.09 (m, 8H), 3.70 (s, 2H, CH_2), 3.81 – 3.90 (m, 6H, OCH_3), 4.01 (s, 3H, OCH_3), 5.26 (s, 2H, CH_2), 6.54 (s, 1H), 6.61 (s, 1H), 7.30 – 7.51 (m, 8H), 7.62 (s, 1H), 8.06 (d, 2H, *J* = 8.2 Hz). ^{13}C-NMR ($CDCl_3$): δ 28.8 (CH_2), 33.7 (CH_2), 51.1 (CH_2), 55.8 (CH_2), 56.0 (OCH_3), 56.0 (OCH_3), 56.7 (OCH_3), 59.7 (CH_2), 71.5 (CH_2), 109.5 (CH), 109.9 (CH), 111.4 (CH), 113.1 (CH), 115.9 (C_q), 120.1 (CH), 126.2 (C_q), 126.4 (C_q), 127.7 (CH), 128.6 (CH), 128.9 (CH), 130.0 (CH), 135.0 (C_q), 135.3 (C_q), 141.8 (C_q), 142.9 (C_q), 147.3 (C_q), 147.6 (C_q), 149.3 (C_q), 152.9 (C_q), 162.1 (CNN). MS *m/z* 206 (100%), 189 (35%), 164 (47%), 146 (36%), 91 (99%), 77 (21%). Molecular composition calculated for $C_{34}H_{34}N_6O_6$: C (65.58%) H (5.50%) N (13.50%), found: C (65.24%) H (5.23%) N (13.22%).

2.3.3. 5-(Benzyloxy)-2-(2-(4-(2-(6,7-dimethoxy-3,4-dihydroisoquinolin-2(1H)-yl)ethyl)phenyl)-2H-tetrazol-5-yl)-4-methoxyaniline (3)—To a stirred solution of compound **2** (1.30 g, 2.09 mmol) in ethanol (30 ml) and tetrahydrofuran (30 ml) under argon, Raney-Nickel (W.R. Grace and Co. Raney®2800 slurry in water, 1 ml) was added. After addition of hydrazine monohydrate (65% aq. solution; 0 h, 5 h, 7.5 h; 1 ml each) the mixture was heated to reflux until no starting material was observed on thin layer chromatography (TLC). The catalyst was filtered off and rinsed with dichloromethane. Evaporation of solvent afforded title compound **3** as white solid (0.94 g, 75%).

^{1}H-NMR ($CDCl_3$): δ 2.79 – 3.11 (m, 8H, CH_2), 3.72 (s, 2H, CH_2), 3.90 – 3.97 (m, 6H, OCH_3), 3.93 (s, 3H, OCH_3), 5.18 (s, 2H, CH_2), 5.25 (bs, 2H, NH_2), 6.36 (s, 1H), 6.54 (s, 1H), 6.61 (s, 1H), 7.29 – 7.51 (m, 7H), 7.74 (s, 1H), 8.08 (d, 2H, *J* = 8.4 Hz). ^{13}C-NMR ($CDCl_3$): δ 28.4 (CH_2), 33.5 (CH_2), 51.0 (CH_2), 55.6 (CH_2), 56.1 (OCH_3), 56.1 (OCH_3), 57.0 (OCH_3), 59.5 (CH_2), 70.8 (CH_2), 101.9 (C_q), 102.6 (CH), 109.6 (CH), 111.5 (CH), 112.2 (CH), 120.0 (CH), 125.9 (C_q), 127.3 (CH), 128.1 (CH), 128.8 (CH), 130.0 (CH), 135.3 (C_q), 136.8 (C_q), 141.4 (C_q), 142.1 (C_q), 142.3 (C_q), 147.5 (C_q), 147.9 (C_q), 151.7 (C_q), 165.0 (CNN). MS *m/z* 592 (M^+, 0.03%), 207 (16%), 206 (100%), 91 (13%), 42 (12%). Molecular composition calculated for $C_{34}H_{36}N_6O_4$: C (68.90%) H (6.12%) N (14.18%), found: C (68.63%) H (5.85%) N (13.97%).

2.3.4. O-benzyl-HM30181 (4)—To an ice cooled solution of compound **3** (0.87 g, 1.47 mmol), 4-oxo-4*H*-chromene-2-carboxylic acid (0.29 g, 1.53 mmol) and 1-hydroxybenzotriazole hydrate (HOBt·H_2O, 14% water, 0.25 g, 1.59 mmol) in DMF (12 ml), ethyl-(*N*′,*N*′-dimethylamino)propylcarbodiimide hydrochloride (EDC·HCl, 0.42 g, 2.19

mmol) was added. After warming to room temperature the reaction mixture was stirred until no starting material was observed on TLC. Upon completion of the reaction, water (48 ml) was added and the mixture was extracted with dichloromethane. The organic fraction was washed with 2M aq. NaOH and brine, dried over Na_2SO_4 and evaporated under vacuum. The crude product was purified by column chromatography (toluene/ethyl acetate/ triethylamine - 7/2/1) to obtain title compound **4** as a yellow solid (0.44 g, 39%).

^{1}H-NMR ($CDCl_3$): δ 2.76 – 3.09 (m, 8H, CH_2), 3.68 (s, 2H, CH_2), 3.83 – 3.89 (m, 6H, OCH_3), 3.97 (s, 3H, OCH_3), 5.23 (s, 2H, CH_2), 6.56 (s, 1H), 6.62 (s, 1H), 7.21 (s, 1H), 7.31 – 7.59 (m, 8H), 7.70 – 7.77 (m, 3H), 8.11 (d, 2H, J = 8.5 Hz), 8.19 (d, 1H, J = 7.9 Hz), 8.66 (s, 1H), 12.45 (s, 1H). ^{13}C-NMR ($CDCl_3$): δ 28.9 (CH_2), 33.8 (CH_2), 51.2 (CH_2), 55.9 (CH_2), 56.1 (OCH_3), 56.1 (OCH_3), 56.4 (OCH_3), 59.7 (CH_2), 70.9 (CH_2), 106.1 (CH), 107.2 (C_q), 109.6 (CH), 110.8 (CH), 111.6 (CH), 112.2 (CH), 118.6 (CH), 120.5 (CH), 124.4 (C_q), 126.0 (CH), 126.2 (C_q), 126.5 (C_q), 128.0 (CH), 128.3 (CH), 128.7 (CH), 130.2 (CH), 131.2 (C_q), 134.7 (CH), 134.9 (C_q), 136.3 (C_q), 143.4 (C_q), 146.5 (C_q), 147.5 (C_q), 147.8 (C_q), 150.7 (C_q), 155.2 (C_q), 155.4 (C_q), 157.4 (C_q), 164.3 (CNN), 178.4 (CON). MS *m/z* 207 (21%), 206 (100%), 164 (35%), 91 (99%), 65 (17%). Molecular composition calculated for $C_{44}H_{40}N_6O_7$: C (69.10%) H (5.27%) N (10.99%), found: C (68.78%) H (5.11%) N (10.67%).

2.3.5. O-desmethyl-HM30181 (5)—To a stirred suspension of **4** (83 mg, 0.11 mmol) in thioanisole (0.83 ml), trifluoroacetic acid (2.65 ml) was added dropwise. Upon complete conversion of the starting material (TLC monitoring) the reaction was neutralised with aq. saturated $NaHCO_3$ solution. The resulting solid was filtered off, washed with toluene and water and dried under vacuum to obtain title compound **5** as a yellow solid (30 mg, 41%).

^{1}H-NMR (d_6-DMSO): δ 2.65 – 3.00 (m, 8H, CH_2), 3.55 (s, 2H, CH_2), 3.65 – 3.76 (m, 6H, OCH_3), 3.88 (s, 3H, OCH_3), 6.57 – 6.73 (m, 2H), 6.95 (s, 1H), 7.43 – 7.71 (m, 5H), 7.77 – 7.91 (m, 1H), 7.97 – 8.13 (m, 4H), 10.12 (bs, 1H), 11.65 (s, 1H, CONH). ^{13}C-NMR (d_6-DMSO): δ 24.5 (CH_2), 29.1 (CH_2), 48.8 (CH_2), 51.2 (CH_2), 55.3 (CH_2), 55.5 (OCH_3), 55.6 (OCH_3), 55.7 (OCH_3), 107.0 (C_q), 109.7 (CH), 110.9 (CH), 111.1 (CH), 111.6 (CH), 118.4 (CH), 120.0 (C_q), 120.2 (CH), 120.5 (CH), 123.4 (C_q), 123.6 (C_q), 125.0 (CH), 126.2 (CH), 129.7 (C_q), 130.3 (CH), 134.7 (C_q), 135.0 (CH), 139.8 (C_q), 145.2 (C_q), 147.7 (C_q), 148.3 (C_q), 149.5 (C_q), 154.8 (C_q), 155.1 (C_q), 156.9 (C_q), 163.5 (CNN), 177.2 (CON). MS *m/z* 207 (25%), 206 (100%), 189 (40%), 164 (70%), 77 (23%). Molecular composition calculated for dihydrochloride $C_{37}H_{34}N_6O_7 \cdot 2HCl \cdot 0.5H_2O$: C (58.73%) H (4.93%) N (11.11%), found: C (58.91%) H (4.95%) N (10.93%).

2.3.6. [^{11}C]HM30181—Using a TracerLab FXC Pro synthesis module, [^{11}C]methyl triflate was bubbled through a solution of radiolabelling precursor **5** (0.5 mg, 0.74 μmol) in DMF (0.1 ml) and acetonitrile (0.4 ml) containing 5 μl of a freshly prepared solution of tetrabutylammonium hydroxide-30 hydrate (TBAH) in methanol (162 mg in 0.5 ml, 2 μmol). After heating for 4 min at 75 °C, the reaction mixture was cooled (25°C), diluted with water (0.5 ml) and injected into a built-in high-performance liquid chromatography (HPLC) system. A Chromolith Performance RP 18-e (100-4.6 mm) column (Merck KGaA, Darmstadt, Germany) was eluted at a flow rate of 5 ml/min with acetonitrile/0.1% aq. trifluoroacetic acid (32/68, v/v). The HPLC eluate was monitored in series for radioactivity and ultraviolet (UV) absorption at a wavelength of 254 nm. Radiolabelling precursor **5** and product [^{11}C]HM30181 eluted with retention times of 3-5 min and 8-12 min, respectively. The product fraction was diluted with water (100 ml) and passed through a C18 Sep-Pak Plus cartridge (Waters Corporation, Milford, USA), which had been preactivated with ethanol (5 ml) and water (10 ml). The cartridge was then rinsed with water (10 ml) followed by elution of [^{11}C]HM30181 with ethanol (3 ml) from the cartridge into a vial containing

Tween 80 (75 μl) and ethanol (0.3 ml). The ethanol was then removed by heating at 90°C under a stream of argon and the product formulated for i.v. injection into animals in 0.9% (w/v) aq. saline at an approximate concentration of 370 MBq/ml. Radiochemical purity and specific activity of [^{11}C]HM30181 were determined by analytical radio-HPLC using a Chromolith Performance RP 18-e (100-4.6 mm) column eluted with acetonitrile/0.1% aq. trifluoroacetic acid (35/65, v/v) at a flow rate of 2 ml/min. UV detection was performed at a wavelength of 240 nm. The retention time of [^{11}C]HM30181 was 6-7 min on this HPLC system. The identity of [^{11}C]HM30181 was confirmed by HPLC coinjection with cold HM30181.

2.3.7. Synthesis of (R)-[^{11}C]verapamil—(*R*)-[^{11}C]verapamil was synthesised as described previously (Brunner et al., 2005). For i.v. injection into animals, (*R*)-[^{11}C]verapamil was formulated in a mixture of phosphate-buffered saline (PBS) and ethanol (9/1, v/v) at an approximate concentration of 370 MBq/ml. Radiochemical purity, as determined by radio-HPLC, was greater than 98% and specific activity at end of synthesis was >100 GBq/μmol.

2.4. Rhodamine 123 efflux inhibition assay

Half-maximum inhibitory concentrations (IC_{50}) were determined in a modification of a previously described method (Chiba et al., 1996). Briefly, cells expressing wild-type Pgp (CCRF-CEM T lymphoblast cell line) were sedimented, the supernatant was removed by aspiration, and the cells were resuspended in Dulbecco's Modified Eagle's Medium (DMEM) containing rhodamine 123 at a final concentration of 0.2 μg/ml (0.53 μM). Cells were loaded with fluorochrome for 30 min at 37°C. Tubes were chilled on ice and cells were harvested at 500 × g in an Eppendorf 5403 centrifuge (Eppendorf, Hamburg, Germany). The cell pellet was washed with ice cold DMEM medium (pH 7.4) and again centrifuged at 500 × g. After resuspension, aliquots of the cell suspension, each containing approximately 1 × 10^6 were transferred to individual fluorescence-activated cell sorter (FACS) tubes and again centrifuged. Supernatants were removed, and the pellets were resuspended individually in prewarmed DMEM medium (pH 7.4) containing either no inhibitor or HM30181 mesylate or elacridar hydrochloride or tariquidar dimesylate at various concentrations in DMSO ranging from 1 to 100 nM. Each inhibitor concentration was measured in duplicate. Right after resuspending cells each individual tube was placed in a temperature controlled unit and cell associated fluorescence was monitored over a period of 5 min with a FACS system (FACSCALIBUR, Becton Dickinson, Vienna, Austria). Exponential curves were fitted to the data points and first order rate constants were determined according to the equation:

$$y=a.e^{-(kt)}+c$$

Whereby y is the fluorescence at time t, a is the initial loading, e is the Euler number, k is the first order rate constant, t is the time in seconds and c is the background fluorescence of cells at infinite time. The first order rate constants k, which are independent of initial loading, were used to generate concentration-response curves from which the IC_{50} values were calculated as 50% occupancy values with Prism 5.0 software (GraphPad Software, La Jolla, USA) using nonlinear regression analysis based on a log-sigmoidal model with fixed slope (Hill slope: −2).

2.5. Experimental design for PET imaging

Two different experimental settings were used in this study. In the first set of experiments, female FVB wild-type mice, aged 8-12 weeks weighing 24±4 g underwent (*R*)-[^{11}C]verapamil PET scans without and with i.v. pretreatment with cold HM30181. Animals

were assigned to 5 groups (n = 4 per group). One group was pretreated with HM30181 vehicle solution (5% aq. glucose solution containing 20 μl 0.01 M aq. HCl) at 60 min before start of the PET scan. The other groups were pretreated with either 10 mg/kg HM30181 at 10, 60 or 120 min before PET or with 21 mg/kg HM30181 at 10 min before PET.

For the second set of experiments, groups of female FVB wild-type, *Mdr1a/b*$^{(-/-)}$, *Bcrp1*$^{(-/-)}$ and *Mdr1a/b*$^{(-/-)}$*Bcrp1*$^{(-/-)}$ mice, aged 11-12 months, weighing 30±3 g underwent [^{11}C]HM30181 PET scans (n = 4 per group).

2.6. PET imaging

Prior to each experiment, the animals were placed in an induction box and anaesthetised with 2.5% isoflurane. During the imaging period anaesthesia was maintained with 1-2% isoflurane administered *via* a cone mask and the isoflurane level was adjusted depending on the depth of anaesthesia. Animal respiratory rate and body temperature were constantly monitored during the data acquisition period (SA Instruments Inc, Stony Brook, NY, USA). The animals were kept warm throughout the experiment at approximately 38°C. Mice were positioned in a custom-made imaging chamber and the lateral tail vain was cannulated for i.v. administration. For PET imaging a microPET Focus220 (Siemens Medical Solutions, Knoxville, USA) was used. Radiotracer ((*R*)-[^{11}C]verapamil: 31±10 MBq; [^{11}C]HM30181: 21±7 MBq, each containing <0.4 nmol of unlabelled compound) was injected over approximately 60 s in a volume of 0.1 ml and dynamic 60-min emission scans were initiated at start of radiotracer injection. After completion of PET imaging, blood was withdrawn from the orbital sinus vein into preweighed micropipettes. Blood samples were weighed and measured for radioactivity in a gamma counter (Perkin Elmer Instruments, Wellesley, USA). Blood radioactivity data were corrected for radioactive decay and expressed as standardised uptake value (SUV=(radioactivity per cubic centimetre/injected radioactivity) × body weight). SUV values can be converted into absolute concentrations values (μg/ml) according to the formula: absolute concentration = SUV × (administered dose (mg)/body weight (kg)) (Bergström et al., 2003).

2.7. PET data analysis

The dynamic emission PET data were sorted into 23 frames, which incrementally increased in time length from 5 s to 10 min. Images were reconstructed using Fourier rebinning of the 3-D sinograms followed by two-dimensional filtered backprojection with a ramp filter resulting in a voxel size of 0.4 × 0.4 × 0.796 mm^3. The standard data correction protocol (normalisation, decay correction and injection decay correction) was applied to the data. For attenuation correction, a corresponding transmission scan using a rotating ^{57}Co point source recorded prior of the PET scan, was used. A calibration factor for converting PET units of the recorded images into radioactivity concentration units was derived by imaging a phantom cylinder filled with a known ^{11}C-radioactivity concentration. Whole brain volumes of interest (VOI) were manually outlined on multiple planes of the PET summation images (0-60 min) using the image analysis software Amide. The VOIs were then transferred to the PET images of the individual time frames to derive time-activity curves, expressed as SUV. Brain uptake of (*R*)-[^{11}C]verapamil and [^{11}C]HM30181 was expressed as the brain-to-blood radioactivity concentration ratio ($K_{b,brain}$) at 60 min after radiotracer injection. $K_{b,brain}$ was calculated by dividing the brain radioactivity concentration in the last PET frame (50-60 min after start of scan) by the blood radioactivity concentration as determined by the gamma counter measurements.

2.8. Analysis of metabolites of [^{11}C]HM30181

A separate group of FVB wild-type mice (n = 3), which did not undergo PET scanning, was injected under isoflurane-anaesthesia with [^{11}C]HM30181 (70±5 MBq in a volume of

approximately 0.1 ml) for metabolite analysis. Animals remained under anaesthesia, were sacrificed at 30 min after radiotracer injection and a terminal blood sample (0.5 ml) was collected. Blood was centrifuged to obtain plasma (10000 × g, 5 min, 21°C), measured for radioactivity in the Wallac gamma counter and analysed for radiolabelled metabolites of [^{11}C]HM30181 using a modified version of a previously described solid-phase extraction assay (Abrahim et al., 2008). In brief, arterial plasma was diluted with water (0.5 ml), spiked with a solution of unlabelled HM30181 in DMSO (10 mg/ml, 20 μl) and acidified with 5M aq. HCl (80 μl) and loaded on a Sep-Pak vac tC18 cartridge (Waters Corporation, Milford, USA), which had been preactivated with methanol (3 ml) and water (5 ml). The cartridge was first washed with water (4 ml) and then eluted with methanol (4 ml). Radioactivity in all three fractions (plasma, water, methanol) was measured in the gamma counter. For validation of the solid-phase extraction assay, [^{11}C]HM30181 dissolved in water (0.5 ml) was subjected to the solid-phase extraction procedure showing that all radioactivity was quantitatively recovered in the methanol fraction.

2.9. In vitro autoradiography

For *in vitro* autoradiography of [^{11}C]HM30181, prefrozen 10-μm tumour sections obtained from female athymic nude NMRI-Foxn1^{nu} mice implanted in one flank with mouse mammary carcinoma cells EMT6 and in the other flank with Pgp overexpressing EMT6Ar1.0 cells as described previously (Wanek et al., 2012) were used. Western blot and immunohistochemical analysis had confirmed Pgp overexpression in EMT6Ar1.0 tumours and only basal Pgp expression levels in EMT6 tumours (Wanek et al., 2012). On the day of the experiment, the tumour sections were thawed and preincubated in PBS. Subsequently, tumour slices were incubated for 30 min with either [^{11}C]HM30181 (62 MBq) and HM30181 vehicle solution (5% glucose solution) or [^{11}C]HM30181 (62 MBq) and unlabelled tariquidar (1 μM) or unlabelled elacridar (1 μM) or unlabelled HM30181 (1 μM). To remove non-specifically bound radiotracer, tumour sections were then washed with cold (4°C) ethanol in PBS (20%, v/v) and distilled water. The sections were air-dried and exposed to a multisensitive phosphor screen (MS, Perkin-Elmer Life Sciences, Waltham, MA, USA). The screens were removed from the film cassettes under dim light conditions and immediately scanned at 600 dpi resolution using a Cyclone storage phosphor system (Perkin-Elmer Life Sciences, Waltham, MA, USA). Images were analysed using the system's Optiquant v5.0 software. Tumours regions of interest were outlined for which the background corrected radioactivity binding (MBq/g) was calculated by using a calibration curve with known ^{11}C-activity concentrations. For comparison, *in vitro* autoradiography was also performed with [^{11}C]tariquidar (Bauer et al., 2010) in presence or absence of unlabelled tariquidar (1 μM) on corresponding EMT6 and EMT6Ar1.0 tumour slices using identical experimental conditions.

2.10. Statistical analysis

Differences between the groups were analysed by one-way analysis of variance (ANOVA) followed by Bonferroni's multiple comparison test using Prism 5.0 software. The level of statistical significance was set to $P<0.05$.

3. Results

3.1. Precursor synthesis and radiosynthesis of [^{11}C]HM30181

The radiolabelling precursor of [^{11}C]HM30181, *O*-desmethyl-HM30181 (**5**), was synthesised following the pathway depicted in Figure 1. 2-Nitro-*O*-benzylvanilline was reacted with 4-methylbenzenesulfonohydrazide to yield derivative **1** which was then reacted with a diazonid in a ring coupling reaction to obtain the corresponding disubstituted tetrazole derivative **2**. The nitro group in **2** was reduced using Raney-Nickel/hydrazine to

yield the corresponding amine **3**. Coupling of **3** with 4-oxo-4*H*-chromene-2-carboxylic acid yielded *O*-benzyl-HM30181 **4**. The benzyl protective group in **4** was removed by reaction with thioanisole and trifluoroacetic acid to give *O*-desmethyl-HM30181 **5**. Precursor **5** was reacted with [^{11}C]methyl triflate to afford [^{11}C]HM30181 in a decay-corrected radiochemical yield of 4.0±1.4% (n = 14), based on [^{11}C]methane, in a total synthesis time of approximately 32 min. Radiochemical purity was greater than 98% and specific activity at end of synthesis was 627±319 GBq/μmol (n = 8).

3.2. Inhibition of rhodamine 123 efflux by HM30181

The inhibitory effect of HM30181 on Pgp-mediated efflux transport of rhodamine 123 was measured in CCRF-CEM T cells and compared with tariquidar and elacridar (Fig. 2). In Figure 2A, representative log concentration-response curves are shown for one experiment in which all three inhibitors were tested using the same cell batch. Figure 2B gives mean (±S.D.) IC_{50} values for all 3 inhibitors from at least 3 independent experiments. The rank order of potency was as follows: elacridar > tariquidar > HM30181.

3.3. Effect of HM30181 on Pgp at the BBB in mice

In order to assess the ability of HM30181 to inhibit Pgp at the murine BBB *in vivo*, we performed PET scans with the Pgp substrate radiotracer (*R*)-[^{11}C]verapamil in FVB wild-type mice without and with i.v. pretreatment with two different doses of cold HM30181 (10 mg/kg and 21 mg/kg, n =4 per group except for the 21 mg/kg dose group where n = 2, Fig. 3). Pretreatment with 10 mg/kg HM30181 was performed at three different time points before injection of (*R*)-[^{11}C]verapamil (10, 60 and 120 min). Brain uptake of *(R)*-[^{11}C]verapamil ($K_{b,brain}$) was not increased in HM30181 pretreated mice compared with vehicle treated mice, irrespective of the time point of HM30181 preadministration or administered dose (Fig. 3B). For comparison, pretreatment of wild-type mice with the Pgp inhibitor tariquidar (15 mg/kg) at 120 min before (*R*)-[^{11}C]verapamil PET had resulted in a 3.7±0.8 fold increase in $K_{b,brain}$ of (*R*)-[^{11}C]verapamil (Fig 3B). Treatment with 21 mg/kg HM30181 caused immediate death in two out of four studied animals and this dose group was therefore discontinued.

3.4. Brain distribution of [^{11}C]HM30181 in wild-type and transporter knockout mice

PET scans with [^{11}C]HM30181 were performed in groups of FVB wild-type, *Mdr1a/b*$^{(-/-)}$, *Bcrp1*$^{(-/-)}$ and *Mdr1a/b*$^{(-/-)}$*Bcrp1*$^{(-/-)}$ mice (n = 4 per group except for *Mdr1a/b*$^{(-/-)}$ where n = 3) (Fig. 4). Blood activity concentrations of [^{11}C]HM30181 at 60 min after injection ranged from 0.1 to 0.2 SUV and were not significantly different in all 4 mouse genotypes. $K_{b,brain}$ of [^{11}C]HM30181 was relatively low and not statistically different between wild-type, *Mdr1a/b*$^{(-/-)}$ and *Bcrp1*$^{(-/-)}$ mice ($K_{b,brain}$: wild-type: 1.9±0.2; *Mdr1a/b*$^{(-/-)}$: 2.8±0.7; *Bcrp1*$^{(-/-)}$: 2.6±0.4) (Fig. 4C). In *Mdr1a/b*$^{(-/-)}$*Bcrp1*$^{(-/-)}$ mice, $K_{b,brain}$ was significantly, i.e. 4.7-fold (P<0.01), 3.2-fold (P<0.05) and 3.4-fold (P<0.01) increased relative to wild-type, *Mdr1a/b*$^{(-/-)}$ and *Bcrp1*$^{(-/-)}$ mice, respectively ($K_{b,brain}$: *Mdr1a/b*$^{(-/-)}$*Bcrp1*$^{(-/-)}$: 8.9±3.8). For comparison, $K_{b,brain}$ of the dual Pgp/Bcrp substrate [^{11}C]tariquidar was 14.5 times higher in *Mdr1a/b*$^{(-/-)}$*Bcrp1*$^{(-/-)}$ mice than in wild-type mice (Fig. 4C).

In a group of wild-type mice which did not undergo PET scanning (n = 3), radiolabelled metabolites of [^{11}C]HM30181 in plasma were analysed using a solid-phase extraction assay. At 30 min after injection of [^{11}C]HM30181, 33±4% of total radioactivity in mouse plasma was in the form of polar radiolabelled metabolites of [^{11}C]HM30181.

3.5. In vitro autoradiography with [^{11}C]HM30181 on Pgp-overexpressing murine breast tumour sections

Figure 5A shows images from *in vitro* autoradiography performed with [^{11}C]HM30181 on low Pgp expressing EMT6 and high Pgp expressing EMT6Ar1.0 tumour sections. Binding of [^{11}C]HM30181 was 1.9 times higher to EMT6Ar1.0 than to EMT6 tumour sections (P<0.001) (Fig. 5B). In EMT6Ar1.0 tumour sections, coincubation with unlabelled tariquidar, elacridar or HM30181 (all 1 μM) significantly reduced [^{11}C]HM30181 binding, i.e. 6.7-fold, 6.3-fold and 2.6-fold (all P<0.001), respectively, as compared with vehicle treated tumour sections. In EMT6 tumour sections, coincubation with tariquidar and elacridar caused significant reduction of [^{11}C]HM30181 binding, by 5.6-fold and 6.1-fold (all P<0.001) respectively, as compared with vehicle treated EMT6 tumour sections. Coincubation with unlabelled HM30181 had no significant effect on [^{11}C]HM30181 binding to EMT6 tumour sections. For comparison, autoradiography was also performed with [^{11}C]tariquidar using the same tumour batches, which displayed 1.8 times higher binding to EMT6Ar1.0 than to EMT6 tumour sections (Fig. 5B insert).

4. Discussion

Inhibition of the multidrug efflux transporter Pgp at the BBB may be a promising approach to facilitate brain entry and thereby improve therapeutic efficacy of CNS targeted drugs (Potschka, 2012). Several Pgp modulators, which were initially developed to treat chemoresistant cancers, were shown to potently inhibit Pgp at the BBB, both in animals and humans (Bauer et al., 2012; Choo et al., 2006; Cutler et al., 2006; Kreisl et al., 2010; Lee et al., 2006). HM30181 is a recently developed Pgp modulator which is currently tested in clinical trials (Kim et al., 2012; Kwak et al., 2010). Presently available *in vitro* data suggest that HM30181 is several times more potent than tariquidar, which is among the most potent Pgp inhibitors known to date (Fox and Bates, 2007), to inhibit Pgp transport *in vitro* (Kwak et al., 2010). Moreover, preclinical data show that oral coadministration of HM30181 (32 mg/kg) significantly enhances the antitumour effect of paclitaxel in mouse brain tumour models (Joo et al., 2008). This was on one hand attributed to the ability of HM30181 to enhance oral bioavailability of paclitaxel by inhibition of intestinal Pgp and on the other hand to inhibition of Pgp-mediated paclitaxel efflux transport at the blood-brain and blood-tumour barriers (Joo et al., 2008).

In search for a PET tracer to visualise Pgp expression levels at the BBB, we studied the ability of HM30181 to inhibit Pgp at the murine BBB by using two different approaches. After having demonstrated that HM30181 was approximately equipotent *in vitro* with tariquidar in the rhodamine 123 efflux inhibition assay (Fig. 2), we investigated, as a first approach, the effect of i.v. HM30181 pretreatment on brain distribution of the radiolabelled Pgp substrate (*R*)-[^{11}C]verapamil in wild-type mice by means of PET imaging (Fig. 3). Previous studies had shown that the third-generation Pgp modulators elacridar and tariquidar were able to enhance brain uptake of (*R*)-[^{11}C]verapamil in rats and mice by several-fold compared with baseline PET scans without inhibitor administration (Kuntner et al., 2010b; Wanek et al., 2012). In contrast to these previous findings, we found no significant effect of HM30181 at doses up to 21 mg/kg (i.v.) on brain uptake of (*R*)-[^{11}C]verapamil (Fig. 3). We were not able to study higher HM30181 doses than 21 mg/kg due to toxicity concerns.

In a second approach, we directly assessed brain distribution of a microdose of ^{11}C-labelled HM30181 (<1 μg) in wild-type and transporter knock-out mice. PET imaging with radiolabelled drugs, also termed PET microdosing, has been proposed as a useful tool to assess distribution of drugs to tissue targeted for treatment (Bergström et al., 2003; Wagner and Langer, 2011). Brain uptake of [^{11}C]HM30181 ($K_{b,brain}$) in wild-type mice was approximately two times higher than brain uptake of [^{11}C]tariquidar (Fig. 4C). Assuming

that a therapeutic dose of HM30181 behaves similarly as a microdose of [^{11}C]HM30181, the brain concentration of [^{11}C]HM30181 measured with PET in wild-type mice (0.5 SUV) (Fig. 4B) would correspond to a concentration of approximately 11 μg/g or 15 μM after administration of 21 mg/kg HM30181. Assuming that HM30181 is a highly protein bound drug (>99%), the unbound concentration of HM30181 would be in the order of 150 nM, which is several times above the drug's *in vitro* IC_{50} for inhibition of rhodamine 123 efflux (13.1±2.3 nM) (Fig. 2B). This argues against the possibility that lack of Pgp inhibitory effect of HM30181 was due to inaccessibility of i.v. administered HM30181 to brain. It should be noted, however, that due to limits in the spatial resolution of small-animal PET (~1 mm), it was not possible to exactly delineate in which tissue compartment radioactivity after i.v. injection of [^{11}C]HM30181 was located (e.g. vascular compartment, brain capillary endothelial cells, brain parenchyma). In humans, maximum plasma concentrations after multiple oral dosing of HM30181 (360 mg) were in the range of 22 ng/ml (Kim et al., 2012), which is several times lower than the blood concentrations achieved in our study in mice at 1 h after i.v. dosing of HM30181 (0.2 SUV corresponding to approximately 4000 ng/ml for the 21 mg/kg dose).

Interestingly, $K_{b,brain}$ of [^{11}C]HM30181 was several times higher in *Mdr1a/b*$^{(-/-)}$*Bcrp1*$^{(-/-)}$ mice as compared with wild-type, *Mdr1a/b*$^{(-/-)}$ and *Bcrp1*$^{(-/-)}$ mice (Fig. 4C), which was consistent with the behaviour of a dual Pgp/Bcrp substrate. There is evidence that many clinically used drugs, notably several tyrosine kinase inhibitors, are dual Pgp/Bcrp substrates (Agarwal et al., 2011). Pgp and Bcrp form a concerted defense mechanism at the BBB, in which one transporter substitutes the other when one is chemically or genetically disrupted (Kodaira et al., 2010). Only when both Pgp and Bcrp are genetically knocked out, dual substrates are able to penetrate the BBB leading to a disproportional increase in brain uptake in combination knockout as compared with single transporter knockout animals.

In order to exclude the possibility that the lack of Pgp inhibitory effect of HM30181 at the murine BBB was caused by rapid *in vivo* metabolism of HM30181, we analysed radiolabelled metabolites of [^{11}C]HM30181 in mouse plasma. It has been reported that the major metabolic pathway for HM30181 in rats was *O*-demethylation of one of the four OCH_3 groups and that *O*-desmethyl-HM30181 was excreted by 50% of the injected dose in faeces at 144 h post dosing (Paek et al., 2006). Our experiments showed that only approximately 30% of total radioactivity in mouse plasma was in the form of polar radiolabelled metabolites of [^{11}C]HM30181 at 30 min after radiotracer injection. It was, however, due to the short radioactive half-life of ^{11}C (20.4 min), not possible to further analyse solid-phase extraction fractions by HPLC to confirm that all radioactivity recovered in the methanol fraction was indeed identical to unchanged [^{11}C]HM30181. Nevertheless our metabolite data suggest that the lack of Pgp inhibitory effect of HM30181 at the murine BBB was in all likelihood not caused by rapid *in vivo* metabolism of HM30181.

A possible explanation for the absence of cerebral Pgp inhibitory effect of HM30181 might be that this drug poorly penetrates cellular membranes. It has been noted before, that the half-maximum effect dose (ED_{50}) of tariquidar to inhibit rhodamine 123 efflux in CD56-positive lymphocytes was 25 times lower than the ED_{50} for enhancement of the brain-to-plasma ratio of loperamide in mice (Choo et al., 2006). This was interpreted in a way that tariquidar first has to diffuse through the cellular membrane before it can reach the Pgp binding site facing the cytosol and that this diffusion barrier might be higher at the BBB than in peripheral cells (Lumen et al., 2010). Similar to tariquidar, the Pgp binding site of HM30181 may be located at a site facing the cytosol, which may be poorly accessible for a large, high molecular-weight molecule, such as HM30181. In line with this assumption it was shown that bioavailability and systemic exposure of orally given HM30181 were very low in humans further supporting that HM30181 is a poorly permeable compound (Kim et

al., 2012). In addition to the relatively poor permeability of HM30181, efflux transport of HM30181 by Pgp and Bcrp at the BBB of wild-type mice might have prevented effective inhibition of cerebral Pgp when assuming that the Pgp inhibitory binding site of HM30181 is different from the substrate binding site. It might thus be possible that higher i.v. doses of HM30181 than those examined in this study (up to 21 mg/kg) would be needed to effectively inhibit Pgp at the BBB.

Based on these data, it appears very unlikely that HM30181 can achieve Pgp inhibition at the BBB at clinically feasible doses. Moreover, [^{11}C]HM30181 does not appear suitable as a PET tracer to assess Pgp density at the BBB. If [^{11}C]HM30181 had shown Pgp specific binding at the murine BBB, PET signal in *Mdr1a/b*$^{(-/-)}$ mice, which lack Pgp at the BBB, would have been decreased rather than increased relative to wild-type animals (Fig. 4C). The *in vivo* behaviour of [^{11}C]HM30181 was similar to that of the previously tested radiolabelled Pgp inhibitors [^{11}C]elacridar and [^{11}C]tariquidar (Bauer et al., 2010; Dörner et al., 2009; Kawamura et al., 2010; Kawamura et al., 2011) suggesting that at microdoses HM30181 is a substrate of both Pgp and Bcrp. This behaviour stands in contrast with earlier published *in vitro* data, suggesting that HM30181 has very high selectivity for Pgp over BCRP (IC_{50} for ATPase inhibition in membrane vesicles: 0.63 nM for Pgp and 3717 nM for BCRP) (Kwak et al., 2010). Moreover, we were not able to confirm that HM30181 was more potent than tariquidar in inhibiting rhodamine 123 efflux *in vitro* (Kwak et al., 2010). In our hands, HM30181 was approximately equipotent with tariquidar in the rhodamine 123 efflux inhibition assay (Fig. 2). In previous work, we had shown that even though [^{11}C]tariquidar was not able to visualise Pgp expression at the murine BBB (Bauer et al., 2010), it could be used to map Pgp expression levels in a murine breast cancer model (Wanek et al., 2012). The suitability of [^{11}C]tariquidar to visualise Pgp expression in tumours, as opposed to the BBB, was explained in a way that Pgp expression levels may have been higher in the tumour model than in brain capillary endothelial cells. Moreover there was only low Bcrp expression in the tumour model, presumably leading to a lesser extent of Bcrp-mediated efflux of [^{11}C]tariquidar in the tumour model than at the BBB (Wanek et al., 2012). Moreover, *in vitro* autoradiography showed higher binding of [^{11}C]tariquidar in high Pgp expressing EMT6Ar1.0 than in low Pgp expressing EMT6 tumours, suggesting that [^{11}C]tariquidar can be used as an *in vitro* radioligand for Pgp density (Wanek et al., 2012). In the present study, we used *in vitro* autoradiography of tumour sections as a further experimental tool to characterise Pgp binding of [^{11}C]HM30181 (Fig. 5). We found that tumour binding of [^{11}C]HM30181 was indeed higher in EMT6Ar1.0 than in EMT6 tumours, to a comparable extent as for [^{11}C]tariquidar (Fig. 5B). In addition, there was a higher degree of [^{11}C]HM30181 binding displacement by cold HM30181 in EMT6Ar1.0 tumours than in EMT6 tumours (Fig. 5B), suggesting that [^{11}C]HM30181 specifically bound to Pgp in the autoradiography set-up. However, our observation that [^{11}C]HM30181 binding was displaced both in EMT6Ar1.0 and EMT6 tumours to a comparable extent by cold elacridar and tariquidar suggests that there may be also a significant degree of non-Pgp specific binding of [^{11}C]HM30181 to tumour sections.

5. Conclusions

Our data show that the novel Pgp modulator HM30181 is not able to inhibit Pgp at the murine BBB at clinically feasible doses suggesting that Pgp at the BBB is considerably less amenable to inhibition as compared with Pgp in peripheral organs. Moreover [^{11}C]HM30181 was found to be unsuitable as a PET tracer to visualise Pgp expression levels at the murine BBB and to behave *in vivo* as a dual substrate of Pgp and Bcrp, comparable to previously characterised [^{11}C]tariquidar. *In vitro* autoradiography, on the other hand, demonstrated some extent of Pgp-specific binding of [^{11}C]HM30181.

Acknowledgments

The research leading to these results has received funding from the Austrian Science Fund (FWF) project "Transmembrane Transporters in Health and Disease" (SFB F35) and the European Community's Seventh Framework Programme (FP7/2007-2013) under grant agreement number 201380 ("Euripides").

References

Abrahim A, Luurtsema G, Bauer M, Karch R, Lubberink M, Pataraia E, Joukhadar C, Kletter K, Lammertsma AA, Baumgartner C, Müller M, Langer O. Peripheral metabolism of (R)-[^{11}C]verapamil in epilepsy patients. Eur. J. Nucl. Med. Mol. Imaging. 2008; 35:116–123. [PubMed: 17846766]

Agarwal S, Hartz AM, Elmquist WF, Bauer B. Breast cancer resistance protein and P-glycoprotein in brain cancer: two gatekeepers team up. Curr. Pharm. Des. 2011; 17:2793–2802. [PubMed: 21827403]

Ashworth PA, Hunjan S, Pretswell IA, Ryder H, Brocchini SJ. Piperazine-2,5-dione derivatives as modulators of multidrug resistance. PCT Int. Appl. 1996 WO 96/20180.

Bang KC, Cha MY, Ahn YG, Ham YJ, Kim MS, Lee GS. P-glycoprotein inhibitor, method for preparing the same and pharmaceutical composition comprising the same. PCT Int. Appl. 2005 WO 2005/033097 A1.

Bankstahl JP, Bankstahl M, Kuntner C, Stanek J, Wanek T, Meier M, Ding X, Müller M, Langer O, Löscher W. A novel PET imaging protocol identifies seizure-induced regional overactivity of P-glycoprotein at the blood-brain barrier. J. Neurosci. 2011; 31:8803–8811. [PubMed: 21677164]

Bauer F, Kuntner C, Bankstahl JP, Wanek T, Bankstahl M, Stanek J, Mairinger S, Dörner B, Löscher W, Müller M, Erker T, Langer O. Synthesis and in vivo evaluation of [^{11}C]tariquidar, a positron emission tomography radiotracer based on a third-generation P-glycoprotein inhibitor. Bioorg. Med. Chem. 2010; 18:5489–5497. [PubMed: 20621487]

Bauer M, Zeitlinger M, Karch R, Matzneller P, Stanek J, Jager W, Bohmdorfer M, Wadsak W, Mitterhauser M, Bankstahl JP, Löscher W, Koepp M, Kuntner C, Müller M, Langer O. Pgp-mediated interaction between (*R*)-[^{11}C]verapamil and tariquidar at the human blood-brain barrier: a comparison with rat data. Clin. Pharmacol. Ther. 2012; 91:227–233. [PubMed: 22166851]

Bergström M, Grahnen A, Långström B. Positron emission tomography microdosing: a new concept with application in tracer and early clinical drug development. Eur. J. Clin. Pharmacol. 2003; 59:357–366. [PubMed: 12937873]

Brandt C, Bethmann K, Gastens AM, Löscher W. The multidrug transporter hypothesis of drug resistance in epilepsy: Proof-of-principle in a rat model of temporal lobe epilepsy. Neurobiol. Dis. 2006; 24:202–211. [PubMed: 16928449]

Brunner M, Langer O, Sunder-Plassmann R, Dobrozemsky G, Müller U, Wadsak W, Krcal A, Karch R, Mannhalter C, Dudczak R, Kletter K, Steiner I, Baumgartner C, Müller M. Influence of functional haplotypes in the drug transporter gene ABCB1 on central nervous system drug distribution in humans. Clin. Pharmacol. Ther. 2005; 78:182–190. [PubMed: 16084852]

Chiba P, Ecker G, Schmid D, Drach J, Tell B, Goldenberg S, Gekeler V. Structural requirements for activity of propafenone-type modulators in P-glycoprotein-mediated multidrug resistance. Mol. Pharmacol. 1996; 49:1122–1130. [PubMed: 8649352]

Choo EF, Kurnik D, Muszkat M, Ohkubo T, Shay SD, Higginbotham JN, Glaeser H, Kim RB, Wood AJ, Wilkinson GR. Differential in vivo sensitivity to inhibition of P-glycoprotein located in lymphocytes, testes, and the blood-brain barrier. J. Pharmacol. Exp. Ther. 2006; 317:1012–1018. [PubMed: 16537797]

Cutler L, Howes C, Deeks NJ, Buck TL, Jeffrey P. Development of a P-glycoprotein knockout model in rodents to define species differences in its functional effect at the blood-brain barrier. J. Pharm. Sci. 2006; 95:1944–1953. [PubMed: 16850390]

Dörner B, Kuntner C, Bankstahl JP, Bankstahl M, Stanek J, Wanek T, Stundner G, Mairinger S, Löscher W, Müller M, Langer O, Erker T. Synthesis and small-animal positron emission tomography evaluation of [^{11}C]-elacridar as a radiotracer to assess the distribution of P-glycoprotein at the blood-brain barrier. J. Med. Chem. 2009; 52:6073–6082. [PubMed: 19711894]

Fox E, Bates SE. Tariquidar (XR9576): a P-glycoprotein drug efflux pump inhibitor. Expert Rev. Anticancer Ther. 2007; 7:447–459. [PubMed: 17428165]

Joo KM, Park K, Kong DS, Song SY, Kim MH, Lee GS, Kim MS, Nam DH. Oral paclitaxel chemotherapy for brain tumors: ideal combination treatment of paclitaxel and P-glycoprotein inhibitor. Oncol. Rep. 2008; 19:17–23. [PubMed: 18097571]

Kannan P, John C, Zoghbi SS, Halldin C, Gottesman MM, Innis RB, Hall MD. Imaging the function of P-glycoprotein with radiotracers: pharmacokinetics and in vivo applications. Clin. Pharmacol. Ther. 2009; 86:368–377. [PubMed: 19625998]

Kannan P, Telu S, Shukla S, Ambudkar SV, Pike VW, Halldin C, Gottesman MM, Innis RB, Hall MD. The “specific” P-glycoprotein inhibitor tariquidar is also a substrate and an inhibitor for breast cancer resistance protein (BCRP/ABCG2). ACS Chem. Neurosci. 2011; 2:82–89. [PubMed: 22778859]

Kawamura K, Konno F, Yui J, Yamasaki T, Hatori A, Yanamoto K, Wakizaka H, Takei M, Nengaki N, Fukumura T, Zhang MR. Synthesis and evaluation of [(11)C]XR9576 to assess the function of drug efflux transporters using PET. Ann. Nucl. Med. 2010; 24:403–412. [PubMed: 20361276]

Kawamura K, Yamasaki T, Konno F, Yui J, Hatori A, Yanamoto K, Wakizaka H, Takei M, Kimura Y, Fukumura T, Zhang MR. Evaluation of Limiting Brain Penetration Related to P-glycoprotein and Breast Cancer Resistance Protein Using [(11)C]GF120918 by PET in Mice. Mol. Imaging Biol. 2011; 13:152–160. [PubMed: 20379788]

Kim TE, Gu N, Yoon SH, Cho JY, Park KM, Shin SG, Jang IJ, Yu KS. Tolerability and pharmacokinetics of a new P-glycoprotein inhibitor, HM30181, in healthy Korean male volunteers: single- and multiple-dose randomized, placebo-controlled studies. Clin. Ther. 2012; 34:482–494. [PubMed: 22284902]

Kodaira H, Kusuhara H, Ushiki J, Fuse E, Sugiyama Y. Kinetic analysis of the cooperation of P-glycoprotein (P-gp/Abcb1) and breast cancer resistance protein (Bcrp/Abcg2) in limiting the brain and testis penetration of erlotinib, flavopiridol, and mitoxantrone. J. Pharmacol. Exp. Ther. 2010; 333:788–796. [PubMed: 20304939]

Kreisl WC, Liow JS, Kimura N, Seneca N, Zoghbi SS, Morse CL, Herscovitch P, Pike VW, Innis RB. P-glycoprotein function at the blood-brain barrier in humans can be quantified with the substrate radiotracer ^{11}C-N-desmethyl-loperamide. J. Nucl. Med. 2010; 51:559–566. [PubMed: 20237038]

Kuntner C, Bankstahl JP, Bankstahl M, Stanek J, Wanek T, Dörner B, Bauer F, Mairinger S, Erker T, Müller M, Löscher W, Langer O. Evaluation of [^{11}C]elacridar and [^{11}C]tariquidar in transporter knockout mice using small-animal PET [symposium abstract]. Neuroimage. 2010a; 52:S25.

Kuntner C, Bankstahl JP, Bankstahl M, Stanek J, Wanek T, Stundner G, Karch R, Brauner R, Meier M, Ding XQ, Müller M, Löscher W, Langer O. Dose-response assessment of tariquidar and elacridar and regional quantification of P-glycoprotein inhibition at the rat blood-brain barrier using (R)-[^{11}C]verapamil PET. Eur. J. Nucl. Med. Mol. Imaging. 2010b; 37:942–953. [PubMed: 20016890]

Kwak JO, Lee SH, Lee GS, Kim MS, Ahn YG, Lee JH, Kim SW, Kim KH, Lee MG. Selective inhibition of MDR1 (ABCB1) by HM30181 increases oral bioavailability and therapeutic efficacy of paclitaxel. Eur. J. Pharmacol. 2010; 627:92–98. [PubMed: 19903471]

Lee YJ, Maeda J, Kusuhara H, Okauchi T, Inaji M, Nagai Y, Obayashi S, Nakao R, Suzuki K, Sugiyama Y, Suhara T. In vivo evaluation of P-glycoprotein function at the blood-brain barrier in nonhuman primates using [^{11}C]verapamil. J. Pharmacol. Exp. Ther. 2006; 316:647–653. [PubMed: 16293715]

Löscher W, Potschka H. Role of drug efflux transporters in the brain for drug disposition and treatment of brain diseases. Prog. Neurobiol. 2005; 76:22–76. [PubMed: 16011870]

Lumen AA, Acharya P, Polli JW, Ayrton A, Ellens H, Bentz J. If the KI is defined by the free energy of binding to P-glycoprotein, which kinetic parameters define the IC50 for the Madin-Darby canine kidney II cell line overexpressing human multidrug resistance 1 confluent cell monolayer? Drug Metabol. Dispos. 2010; 38:260–269.

Luurtsema G, Schuit RC, Klok RP, Verbeek J, Leysen JE, Lammertsma AA, Windhorst AD. Evaluation of [^{11}C]laniquidar as a tracer of P-glycoprotein: radiosynthesis and biodistribution in rats. Nucl. Med. Biol. 2009; 36:643–649. [PubMed: 19647170]

Mairinger S, Erker T, Müller M, Langer O. PET and SPECT radiotracers to assess function and expression of ABC transporters in vivo. Curr. Drug Metabol. 2011; 12:774–792.

O'Brien FE, Dinan TG, Griffin BT, Cryan JF. Interactions between antidepressants and P-glycoprotein at the blood-brain barrier: clinical significance of in vitro and in vivo findings. Br. J. Pharmacol. 2012; 165:289–312. [PubMed: 21718296]

Paek IB, Ji HY, Kim MS, Lee G, Lee HS. Metabolism of a new P-glycoprotein inhibitor HM-30181 in rats using liquid chromatography/electrospray mass spectrometry. Rapid Commun. Mass Spectrom. 2006; 20:1457–1462. [PubMed: 16586459]

Potschka H. Role of CNS efflux drug transporters in antiepileptic drug delivery: Overcoming CNS efflux drug transport. Adv. Drug. Deliv. Rev. 2012 doi:10.1016/j.addr.2011.12.007.

Sharp MJ, Mader CJ, Strachan C. Synthesis of acridine derivate multidrug-resistant inhibitors. PCT Int. Appl. 1998 WO 98/52923 A1.

Spudich A, Kilic E, Xing H, Kilic U, Rentsch KM, Wunderli-Allenspach H, Bassetti CL, Hermann DM. Inhibition of multidrug resistance transporter-1 facilitates neuroprotective therapies after focal cerebral ischemia. Nat. Neurosci. 2006; 9:487–488. [PubMed: 16565717]

van Vliet EA, van Schaik R, Edelbroek PM, Redeker S, Aronica E, Wadman WJ, Marchi N, Vezzani A, Gorter JA. Inhibition of the multidrug transporter P-glycoprotein improves seizure control in phenytoin-treated chronic epileptic rats. Epilepsia. 2006; 47:672–680. [PubMed: 16650133]

Wagner CC, Langer O. Approaches using molecular imaging technology - use of PET in clinical microdose studies. Adv. Drug. Deliv. Rev. 2011; 63:539–546. [PubMed: 20887762]

Wanek T, Kuntner C, Bankstahl JP, Bankstahl M, Stanek J, Sauberer M, Mairinger S, Strommer S, Wacheck V, Löscher W, Erker T, Müller M, Langer O. A comparative small-animal PET evaluation of [^{11}C]tariquidar, [^{11}C]elacridar and (R)-[^{11}C]verapamil for detection of P-glycoprotein-expressing murine breast cancer. Eur. J. Nucl. Med. Mol. Imaging. 2012; 39:149–159. [PubMed: 21983837]

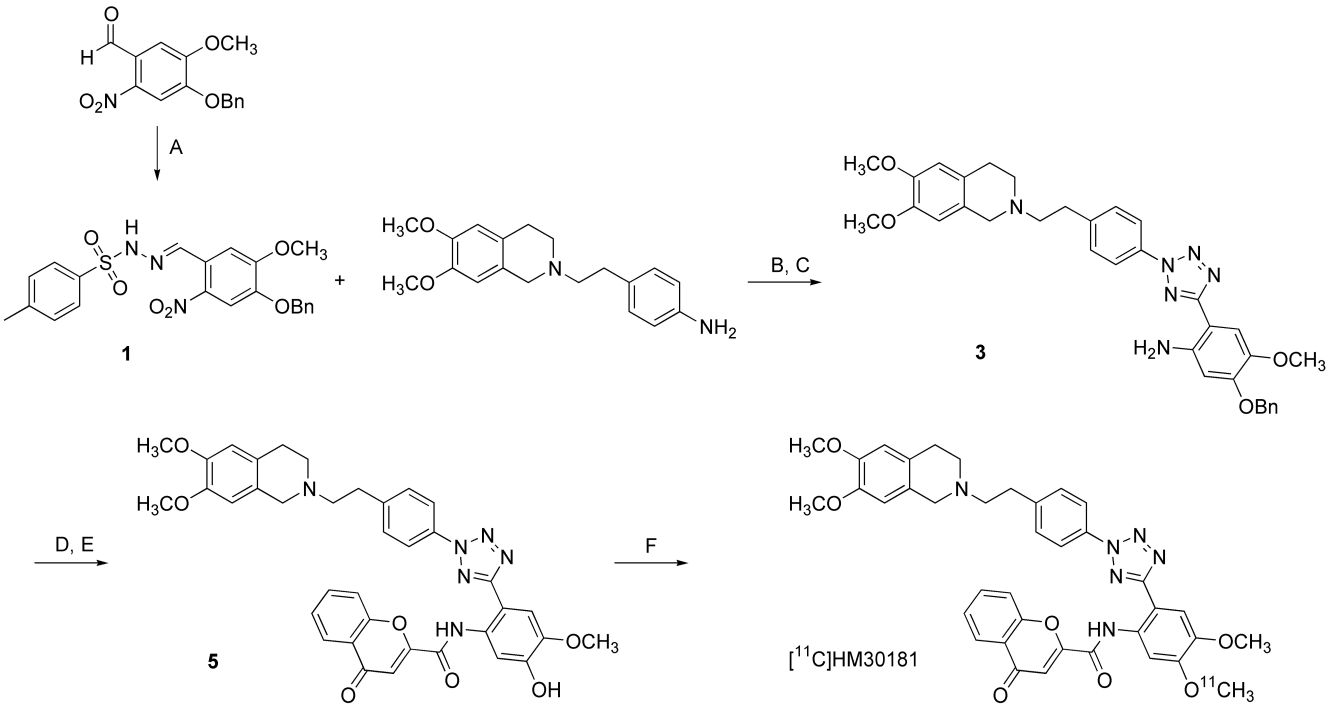

Fig. 1.

Synthesis of *O*-desmethyl-HM30181 (**5**) and [^{11}C]HM30181 by [^{11}C]methylation with [^{11}C]methyl triflate. Reagents: (A) 4-methylbenzenesulfonohydrazide, ethanol, reflux; (B) $NaNO_2$, aq. HCl, ethanol, pyridine, 0°C to −15°C; (C) Raney-Nickel, $(NH_2)_2{\cdot}H_2O$, tetrahydrofuran/ethanol, reflux; (D) 4-oxo-4*H*-chromene-2-carboxylic acid, HOBt, EDC·HCl, DMF, 0°C to room temperature; (E) trifluoroacetic acid, thioanisole, room temperature; (F) [^{11}C]methyl triflate, TBAH, DMF/acetonitrile, 75°C.

Europe PMC Funders Author Manuscripts

Europe PMC Funders Author Manuscripts

A

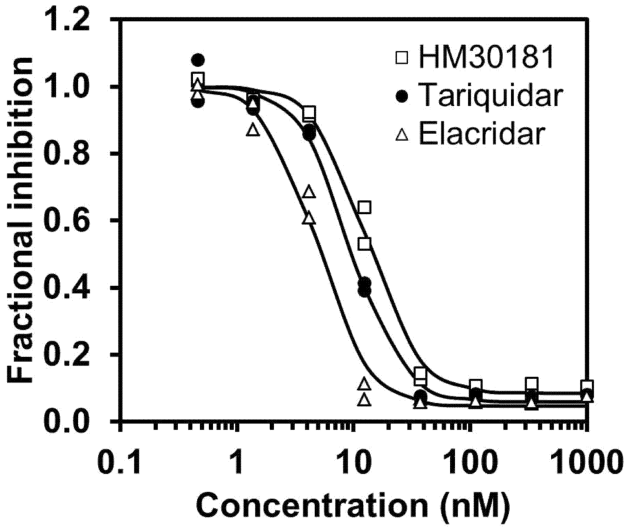

B

	IC_{50}, nM (mean±S.D.)	cLog *P*
HM30181	13.1±2.3	7.87±0.79
Tariquidar	8.2±2.0	6.38±0.81
Elacridar	5.2±0.6	5.55±1.38

Fig. 2.

(A) Representative log concentration-response curves for inhibition of Pgp-mediated efflux transport of rhodamine 123 from CCRF-CEM T lymphoblast cells for HM30181, tariquidar and elacridar (1-100 nM). Response is expressed as fractional inhibition relative to experiment without inhibitor. All experiments were performed in duplicate and the same cell batch was used for assessment of all three inhibitors. Nonlinear regression analysis based on a log-sigmoidal model with fixed slope (Hill slope: -2) was performed using Prism 5.0 software. (B) Mean (±S.D.) half-maximum inhibitory concentrations (IC_{50}, nM) of HM30181, tariquidar and elacridar in the rhodamine 123 efflux inhibition assay from at least 3 independent experiments performed each in duplicate and calculated log *P* values (*P* = octanol-to-water partition coefficient) using ACD/Labs ChemSketch 12.01 (Toronto, Canada).

Europe PMC Funders Author Manuscripts

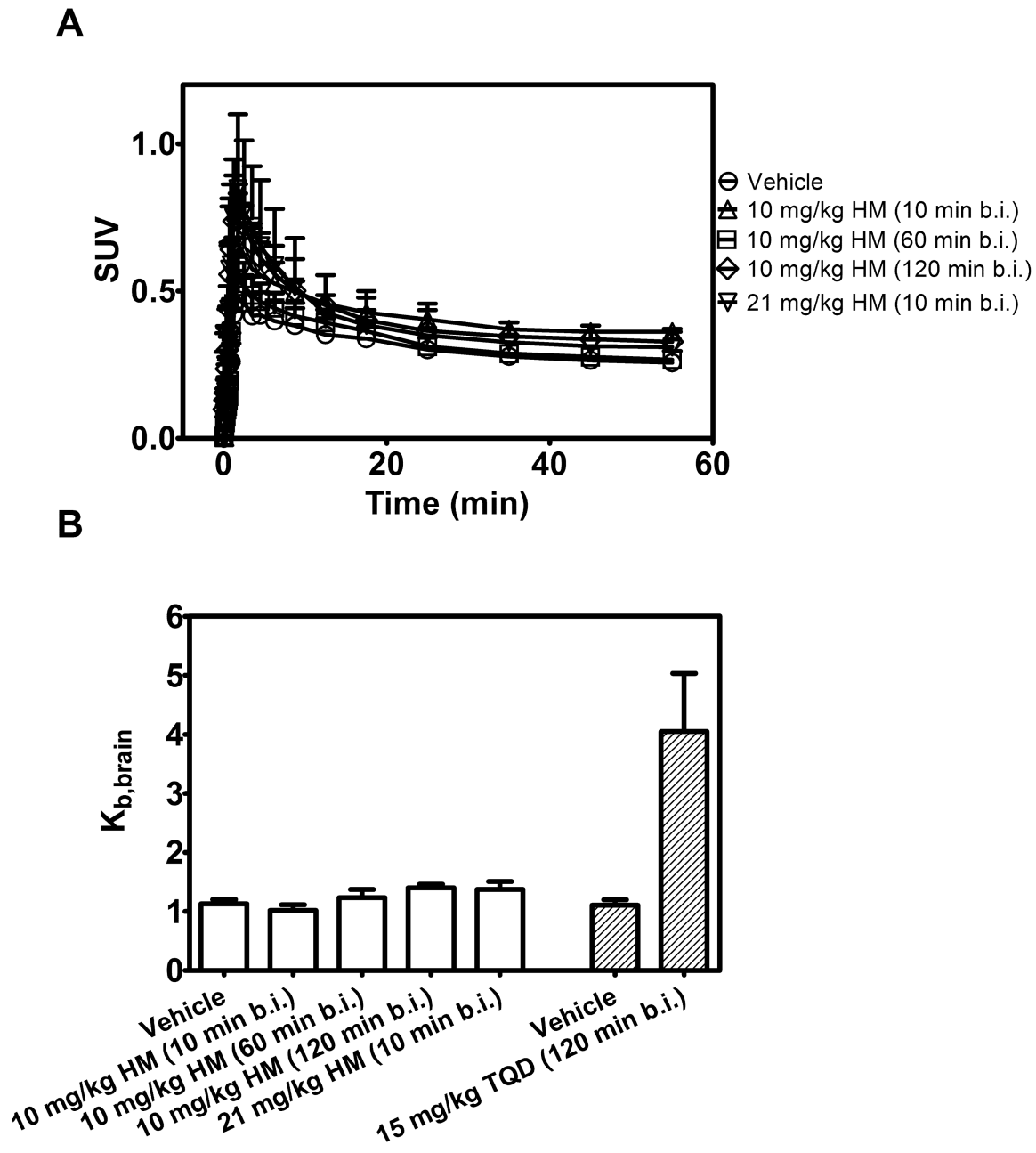

Fig. 3.

(A) Mean (+S.D.) brain time-activity curves of (*R*)-[^{11}C]verapamil in FVB wild-type mice pretreated i.v. with vehicle solution (at 60 min before PET) or HM30181 (HM, 10 mg/kg at 10, 60 or 120 min before PET or 21 mg/kg at 10 min before PET, $n = 4$ per group except for 21 mg/kg dose group where $n = 2$). In (B) mean (+S.D.) brain-to-blood radioactivity concentration ratios at the end of the PET scan ($K_{b,brain}$) are shown. For comparison, $K_{b,brain}$ of (*R*)-[^{11}C]verapamil in FVB wild-type mice pretreated with vehicle or tariquidar (15 mg/kg) at 120 min before PET is also shown (Kuntner et al., 2010a).

Europe PMC Funders Author Manuscripts

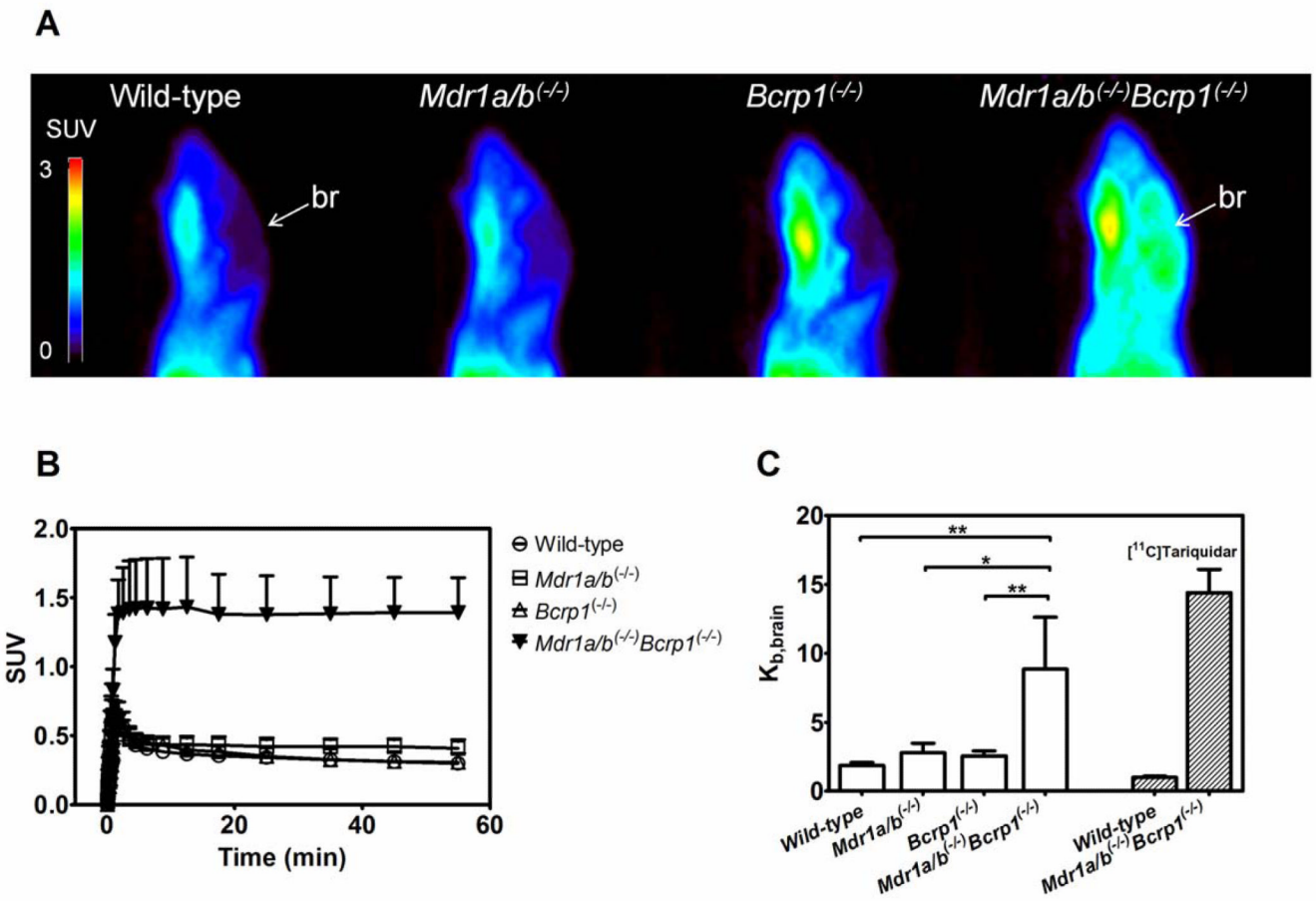

Fig. 4.

Sagittal PET summation images (0-60 min) (A) and mean (+S.D.) brain time-activity curves (B) of [^{11}C]HM30181 in FVB wild-type, *Mdr1a/b*$^{(-/-)}$, *Bcrp1*$^{(-/-)}$ and *Mdr1a/b*$^{(-/-)}$*Bcrp1*$^{(-/-)}$ mice (n = 4 per group except for *Mdr1a/b*$^{(-/-)}$ where n = 3). All images are set to the same intensity scale (0-3 SUV). The localisation of the brain (br) is indicated by a white arrow. In (C) mean (+S.D.) brain-to-blood radioactivity concentration ratios at the end of the PET scan ($K_{b,brain}$) are shown (*, P<0.05, **, P<0.01, 1-way ANOVA followed by Bonferroni's multiple comparison test). For comparison, $K_{b,brain}$ of [^{11}C]tariquidar in FVB wild-type mice and in *Mdr1a/b*$^{(-/-)}$*Bcrp1*$^{(-/-)}$ is also shown (Bauer et al., 2010).

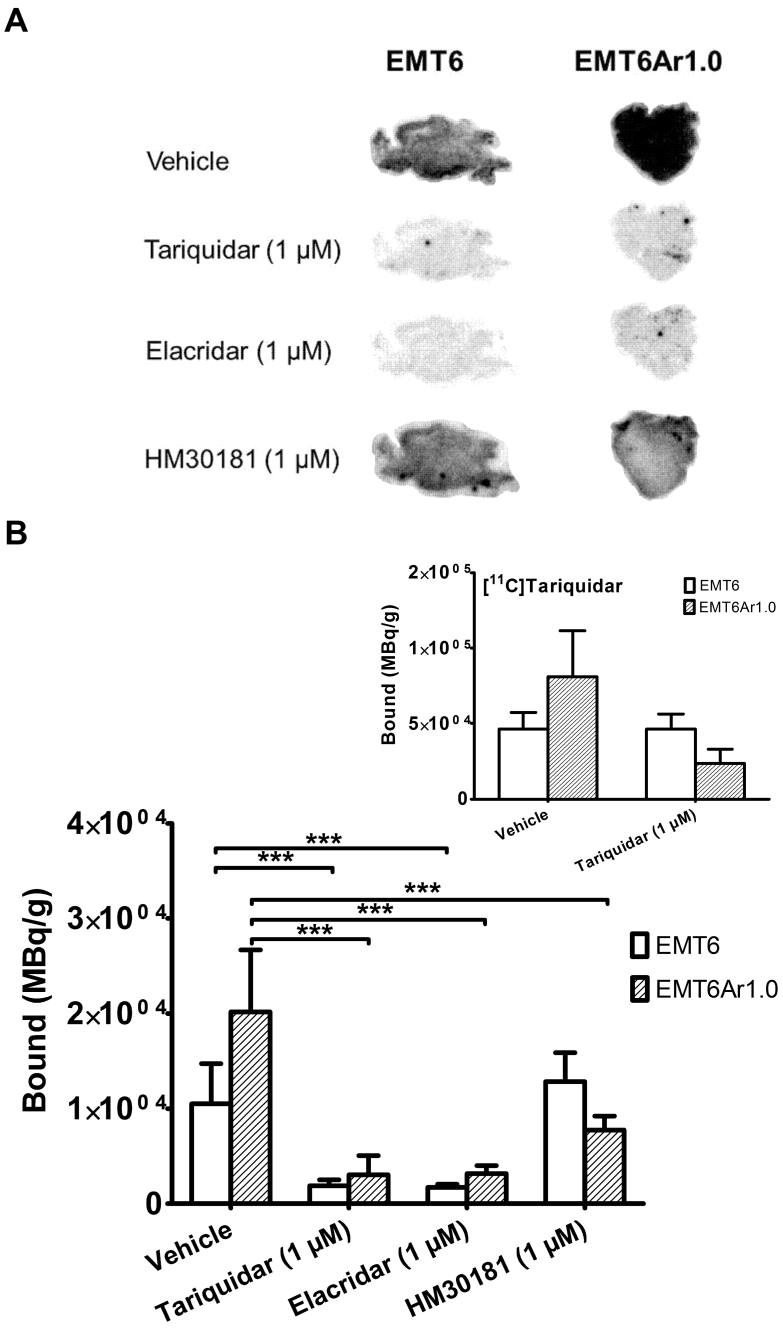

Fig. 5.

(A) Autoradiography images obtained after incubation of EMT6 and EMT6Ar1.0 tumour slices with [^{11}C]HM30181 alone (in 5% glucose solution, vehicle) or [^{11}C]HM30181 in presence of cold tariquidar, elacridar or HM30181 (all 1 μM). (B) Quantitative assessment of the autoradiography images in bound MBq per gram tumour (mean+S.D., n = 3-6 for each condition, ***, P<0.001, 1-way ANOVA followed by Bonferroni's multiple comparison test). For comparison, binding of [^{11}C]tariquidar (without and with 1 μM unlabelled tariquidar) to the same batch of EMT6 and EMT6Ar1.0 tumour slices is shown as insert.